Research Article

Journal of RAMAN SPECTROSCOPY

Received: 22 April 2011 Revised: 20 July 2011 Accepted: 21 July 2011 Published online in Wiley Online Library: 27 October 2011

(wileyonlinelibrary.com) DOI 10.1002/jrs.3057

Raman spectroscopic characterization of the magnesium content in amorphous calcium carbonates

Dongbo Wang, Laura M. Hamm, Robert J. Bodnar and Patricia M. Dove*

A series of Mg-bearing synthetic amorphous calcium carbonates (ACC) were characterized by Raman spectroscopy. The spectra showed a systematic increase in the carbonate ν_1 peak position from the control samples that contained 0.0 mol % $MgCO_3$ to samples that contained up to 43 mol % $MgCO_3$. The relationship is best described by the function: mol % $MgCO_3 = (\nu_1 - 1079.66) / 0.2017$. The Mg content is equally well-predicted by a correlation with the instrumentally corrected ν_1 full width at half maximum that is quantified by: mol % $MgCO_3 = (\nu_1 - 23.26) / 0.1969$. An analysis of the Raman data collected for ACC combined with insights from crystalline materials suggests that compositional dependencies arise from changes in the local metal–oxygen bonds as Mg substitutes for Ca. The calibrations described here provide a rapid and nondestructive means of determining the Mg content of ACC, with additional advantages of minimal sample preparation and a high degree of lateral spatial resolution (approximately 1 μm). This method may be appropriate for investigations of heterogeneous samples such as biominerals. Copyright © 2011 John Wiley & Sons, Ltd.

Supporting information can be found in the online version of this article.

Keywords: biomineralization; precursor; calibration; calcite

Introduction

With the realization that amorphous calcium carbonates (ACC) are ubiquitous in biomineralizing environments,[1] the formation and transformation of this reactive intermediate phase into crystalline products has become the focus of recent research in carbonate biomineralization.[1–9] *In vitro* and *in vivo* investigations of calcification processes show that ACC acts as a 'moldable' precursor that is essential for the formation of complex hierarchical assemblages. Moreover, ACC provides a means of storing Ca^{2+} and CO_3^{2-} ions until these constituents are needed for rapid mineralization.[6,10] As a result, carbonate biomineralizing systems are able to produce functional materials of complex morphologies and enhanced mechanical properties.

One factor that greatly influences ACC stability and its transformation to a crystalline phase is magnesium (Mg) content.[11,12] Magnesium is commonly found in biological systems at relatively high concentrations and, additionally, modern seawater contains five times more Mg than Ca.[13] A recent study shows calcifying eukaryotic organisms use Mg to regulate the kinetics and pathway of mineralization by slowing the ACC to crystalline transformation.[5] Despite the newly recognized importance of Mg in regulating ACC formation and crystallization, there are few reports of the Mg contents of ACC from biological tissues or environmental samples. This deficiency is likely because a simple chemical probe with a high spatial resolution that is specifically sensitive to ACC has not yet been developed. One limitation to developing such a probe is the overwhelmingly strong signature of crystalline components observed using standard bulk characterization techniques, such as X-Ray Diffraction (XRD) and aqueous analyses (inductively coupled plasma-mass spectrometry/optical emission spectroscopy or atomic absorption spectroscopy). Here, we show that Raman spectroscopy can be used to determine the Mg content of ACC. This approach offers significant advantages for ACC analysis because it is a rapid, nondestructive technique that requires minimal sample preparation and provides a high lateral spatial resolution (approximately 1 μm) and a small analytical volume (~1–10 μm^3).

There are six common phases of calcium carbonate, of which three are anhydrous crystalline phases, commonly found in biominerals: calcite, aragonite, and vaterite. The three others are hydrated, two of which are crystalline and only found in geological samples: monohydrocalcite and ikaite.[14] Finally, there is ACC, which normally exists as an amorphous monohydrate.[15] Calcite is the only crystalline form of calcium carbonate that accommodates substantial amounts of structural Mg,[16–18] where Mg contents of up to 25 mol % are common. The crystalline carbonates typically exhibit six vibrational modes by Raman spectroscopy (Table 1). Two of the vibrations are lattice modes, observable in all crystalline carbonates (a translation mode, and a higher frequency libration) but not in ACC. The carbonate ion has four internal modes, although only two modes are known to be observable in ACC: the symmetric C–O stretch (ν_1) and an antisymmetric stretch (ν_3).[14]

A recent Raman spectroscopic study correlated the Mg concentration in calcite with peak position.[19] We use a similar approach to relate the symmetric stretch (ν_1) peak position and the full width at half maximum (FWHM) of the ν_1 peak to the Mg content

* *Correspondence to: Patricia Dove, Department of Geosciences, Virginia Tech, Blacksburg, VA 24061, USA.*
E-mail: dove@vt.edu

Department of Geosciences, Virginia Tech, Blacksburg, VA, 24061, USA

Table 1. Summary of peak positions for Raman active modes in calcite, dolomite, magnesite[27] and ACC (this study)

Carbonate phase		Calcite	Dolomite	Magnesite	ACC
	Raman active modes	Peak position (cm^{-1})			
Lattice	Translation	154	175	213	—
	Libration	281	299	329	—
Internal	ν_1 (symmetric)	1085	1097	1094	1080
	ν_2 (out of plane bend)	1748	1750	1762	—
	ν_3 (antisymmetric)	1434	1439	1444	—
	ν_4 (in-plane bend)	711	724	738	714

of ACC. Because of the absence of the Raman lattice modes in ACC, the strongest carbonate internal mode (ν_1, symmetric stretch) is characterized in this study. The resulting relationship between the Mg content in ACC and the Raman spectral properties holds promise for applications in heterogeneous biological and environmental specimens where the simultaneous identification of the phase and determination of its Mg content in ACC is desired.

Experimental

Amorphous calcium carbonate was synthesized using the standard ammonium carbonate diffusion method.[2,20] Samples of Mg-containing ACC were produced using solutions with Mg/Ca ratios of 0 to 10 by holding [Ca^{2+}] constant at 25 mM ($CaCl_2$, 99.9%; Sigma) and adjusting Mg concentrations accordingly ($MgCl_2$, 99.9%; Sigma). The solution (6.0 mL) was pipetted into a glass Petri dish and then sealed in a desiccator with 0.6–0.7 g of ammonium carbonate salt [$(NH_4)_2CO_3$; Sigma]. For each solution Mg/Ca ratio, three replicates were prepared from single solutions for both compositional analysis and corresponding Raman analyses.

To prepare each ACC sample, acid/peroxide washed glass slides were placed in glass Petri dishes. The solutions were then introduced and incubated with ammonium carbonate. Each experiment was carefully monitored until the solutions became visibly cloudy, after which the glass slides were removed and washed in anhydrous ethanol (99.5%; Sigma). Then samples were dried and stored under vacuum until Raman analysis. The remaining solution with suspended ACC was prepared for chemical analysis by filtering the solutions through 0.2 μM nylon membranes (Whatman). The filtrate was then rinsed in anhydrous ethanol and dried overnight under vacuum. The filter membranes were placed in 0.1 M nitric acid (99.999%; Sigma) for 30 min and then removed prior to analysis by inductively coupled plasma–optical emission spectrometry (ICP–OES) using a Spectro CirOS VISION. The Mg and Ca concentrations were determined from calibration curves that were prepared from plasma-grade single element standards (SPEX CertiPreps).

The Mg and Ca molar concentrations of ACC measured by ICP–OES were converted into mol % $MgCO_3$ by assuming the stoichiometry:[2]

$$y\mathrm{Mg}^{2+} + z\mathrm{Ca}^{2+} + (y+z)(\mathrm{CO_3}^{2-}) = (\mathrm{Ca}_z\mathrm{Mg}_y(\mathrm{CO_3})_{y+z}) \quad (1)$$

where mol % $MgCO_3$ is given by $y/(y+z)$*100. The resulting materials contained 0.0 to approximately 43 mol % $MgCO_3$.

Raman spectra were acquired for each of the corresponding samples using a JY Horiba LabRam (800 mm) HR spectrometer equipped with a 632.81 nm He–Ne laser emitting 15 mW power at the source and focused through an Olympus 100× objective (Numerical aperture (NA) = 0.9). The spectrograph had a 600 grooves/mm grating and spectra were collected with a 150 μm slit width and 400 μm confocal aperture setting. The detector was a Peltier-cooled charge coupled device with 1024 × 256 pixels, optimally operating at −70 °C. The spectral window corresponding to the grating and detector characteristics was approximately 1000 cm^{-1}. Three 180s spectra accumulations were collected and averaged for each of the samples analyzed and reported in this study. Corrections for drift and nonlinearity of the spectrometer were performed to obtain true peak positions. Two Ne emission lines at 914.90 cm^{-1} and 1371.26 cm^{-1} bounding the ν_1 peak of the carbonate were simultaneously collected with every ACC spectrum, as shown in Fig. 1. The measured position of the ν_1 peak for carbonate was corrected using the known positions of the Ne lines according to:

$$\nu_{1,\,\mathrm{corrected}}^{\mathrm{carbonate}} = \frac{1}{2}\left\{\left[\nu_{1,\,\mathrm{measured}}^{\mathrm{carbonate}} + \left(\nu_{\mathrm{standard}}^{\mathrm{Ne,914.90}} - \nu_{\mathrm{measured}}^{\mathrm{Ne,914.90}}\right)\right] + \left[\nu_{1,\,\mathrm{measured}}^{\mathrm{carbonate}} + \left(\nu_{\mathrm{standard}}^{\mathrm{Ne,1371.28}} - \nu_{\mathrm{measured}}^{\mathrm{Ne,1371.28}}\right)\right]\right\} \quad (2)$$

As noted by other workers, Raman peaks will show some variability in measured position over time as the laser intensity, microscope focus, temperature in the laboratory, etc. varies.[21,22] In our study, the observed positions of the Ne emission lines drifted to higher wavenumbers during the course of our experiments. We observed shifts of up to one wavenumber over 12 h, demonstrating the necessity to collect reference Raman lines simultaneously with the spectrum of the unknown (ACC) to compare and correlate Raman peak positions measured at different times within a single analytical session and in different analytical sessions. The collection of Ne reference lines simultaneously with each ACC spectrum was also necessary to develop a calibration equation that is instrument-independent and is transportable between laboratories. While the measured positions of the individual Ne lines vary during an analytical session for the reasons mentioned above, the difference in peak positions remained constant at 456.3 $cm^{-1} \pm 0.09$, which suggests that the linear interpolation used in Eqn (2) above is valid. It should also be noted that in an earlier study in this laboratory in which two other Ne lines were used for peak position calibration, a total of 231 analyses of the peak positions were made, and the measured position of the higher wavenumber Ne line varied from 2972.91 cm^{-1} to 2972.44 cm^{-1}, or a range of 0.47 cm^{-1}. Similarly, the measured position of the lower wavenumber Ne line ranged from 2851.86 cm^{-1} to 2851.40 cm^{-1}, for a total variation of 0.46 cm^{-1}. However, the difference in peak positions showed a range of only 0.05 cm^{-1}, with a standard deviation of 0.012 cm^{-1}.[21,22]

The Ne peak positions and the carbonate peak positions and widths were estimated using a summed Gaussian/Lorentzian peak-fitting routine after baseline corrections were made using the Jobin Yvon LabSpec version 4 software. A neon calibration lamp (model 6032, Newport Instruments) positioned within the optical path of the Raman spectrometer made it possible to collect the Raman spectra for the Ne calibration lines and for the ACC simultaneously.

It is well known that Raman measurements such as FWHM are instrument-dependent. However, if the instrument parameters are known, it is possible to correct the measured FWHM to obtain a real (or corrected) FWHM that can then be used to compare results from different instruments.[23] This approach has been applied successfully to the study of metamictisation of zircon

Journal of RAMAN SPECTROSCOPY

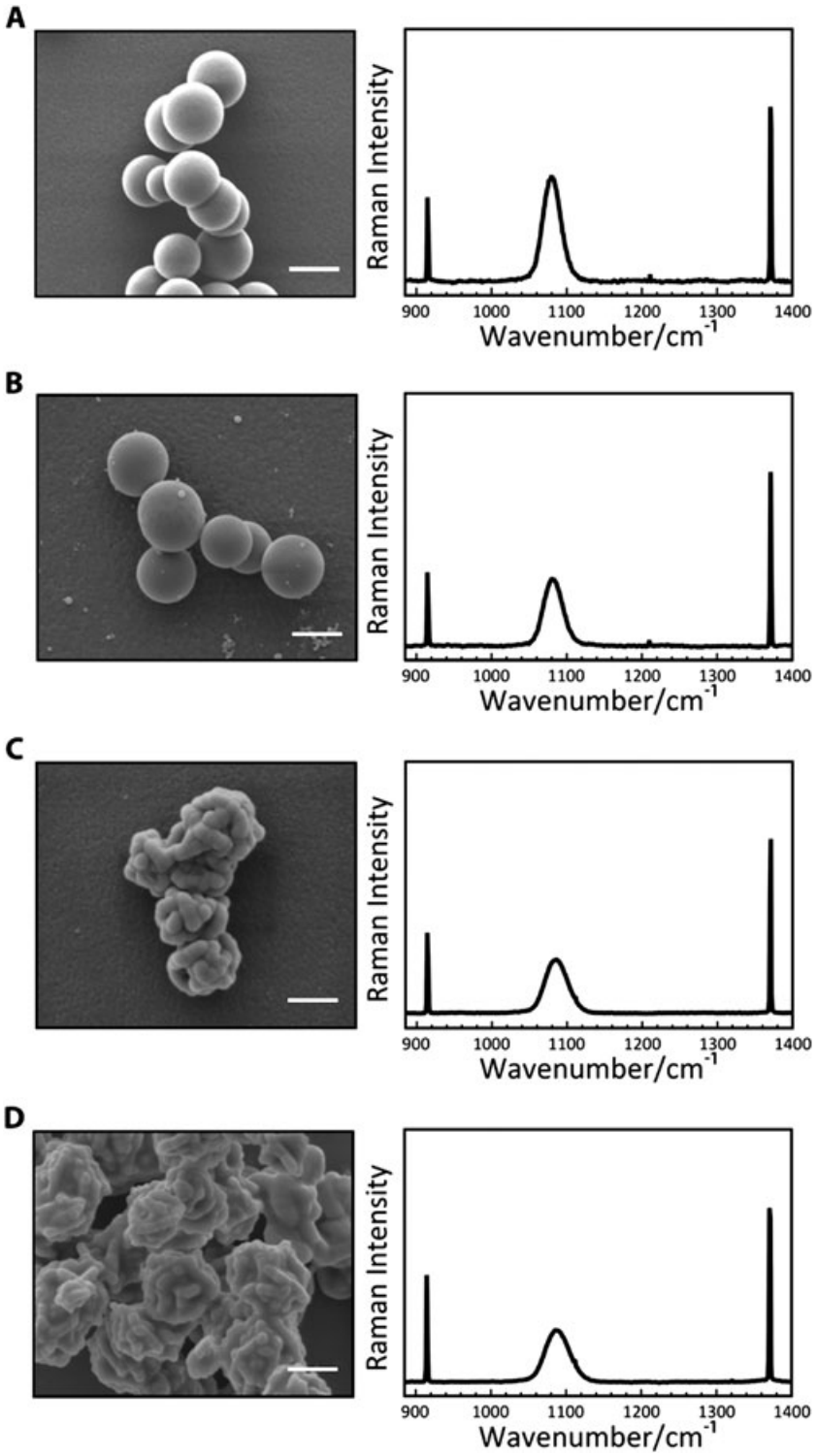

Figure 1. Scanning electron microscopy images show the characteristic morphologies of ACC precipitates with the corresponding Raman spectra of carbonate ν_1 peak (center) and Ne emission lines at 914.90 cm^{-1} and 1371.26 cm^{-1}. (a) ACC that contains 0 mol % $MgCO_3$; (b) ACC with 10 mol % $MgCO_3$; (c) ACC with 34 mol % $MgCO_3$; and (d) ACC with 43 mol % $MgCO_3$. All scale bars = 1 μm.

crystals.[24] Nasdala *et al.*[24] described a simplified equation for determining the true FWHM from measured data,

$$b = b_s \bullet \sqrt{1\text{-}2\left(\frac{s}{b_s}\right)^2}$$

where b is the corrected FWHM, b_s is the measured FWHM and s is the apparatus function. The apparatus function is determined by measuring the FWHM for a peak with a known (theoretical) FWHM and comparing the two values (L. Nasdala, personal comm., 2010). In this study, the FWHM of the diamond peak nominally located at 1332 cm^{-1} and with a known FWHM

of ~1.6 cm^{-1}[25] was used to determine the apparatus function. The measured FWHM of the 1332 cm^{-1} peak, obtained using a LabRam HR (800 mm) spectrometer with 600 grooves/mm grating and 632.81 nm excitation wavelength, was ~3.7 cm^{-1}, resulting in an apparatus function of 2.3. Generally, the corrected peak widths (b) can be considered to be reliable as long as $b \geq 2s$.[24] In this study the corrected FWHM values (b) ranged from ~23 to 33, or approximately 10–14 times greater than the value for the apparatus function, s. All FWHM are presented as corrected measurements.

Results

Representative morphologies of ACC materials that contain 0–43 mol% $MgCO_3$ are shown in Figs 1(a)–(d). Mg-free ACC is comprised of discrete spherical particles (Fig. 1(a)). This morphology is maintained over the compositional range from 0 to 10 mol % $MgCO_3$ (solution Mg/Ca = 2) and perhaps higher (Fig. 1(b)). As the Mg content of ACC increases to 34 mol % $MgCO_3$ (Fig. 1(c)) (solution Mg/Ca = 5) and 43 mol % $MgCO_3$ (Fig. 1(d)) (solution Mg/Ca = 10), the morphology evolves to produce a texture comprised of smaller aggregated particles. The change in morphology with increasing Mg content is consistent with a previous investigation that showed that ACC with $MgCO_3$ contents >20 mol % exists as coalesced particles.[26]

The corresponding Raman spectra for the ACC shown in Figs 1(a)–(d) have systematic shifts in peak position, FWHM, and intensity with increasing Mg content. These variations form the basis for the correlation reported here. The measured Raman shifts are also consistent with analyses of Mg-bearing calcites that show a decrease in peak intensity, peak broadening and red shifts in the Raman ν_1 carbonate symmetric stretch[27] with increasing Mg content.

To establish the correlation between the Mg content of ACC and Raman spectral properties, we first determined the ν_1 peak position of the Mg-free control materials. The average corrected peak position of the ν_1 band was 1079.87 cm^{-1} +/− 0.04 cm^{-1}, where $n = 3$. This position is in general agreement with the literature values of 1077 cm^{-1} in synthetic samples.[14] We combined the control measurements of the ν_1 peak with the analyses of the Mg-bearing ACC materials to obtain the relationship shown in Fig. 2. A linear regression fit of the ν_1 peak positions to the measured $MgCO_3$ contents gives the following relationship:

$$\text{mol \% MgCO}_3 = \frac{\nu_1 - b}{m} \quad (3)$$

where the b (intercept) and m (slope) parameters of Eqn (3) are listed in Table 2. Proportional error based on Raman measurements gives the relationship[28]

$$\text{error mol \% MgCO}_3 = \nu_1 \sqrt{\left(\frac{s_m}{m}\right)^2 + \left(\frac{s_b}{b}\right)^2} \quad (4)$$

and values for s_m and s_b are tabulated in Table 2.

Further analysis of the data shows that the FWHM of the ν_1 peak is related to the peak position (Fig. S1) and may provide an equally useful predictor of Mg content in ACC. For those who were unable to collect Raman spectra for peak position calibration lines (i.e. using Ne, Hg, or Ar lines) simultaneously with the spectrum for the ACC, the FWHM calibration may be preferred because peak width is independent of peak position, although it can be instrument-dependent. The linear regression fit of FWHM *versus* mol % $MgCO_3$ in ACC (Fig. 3 and Table 2) yields a coefficient of determination equal to 0.947, a value identical to that obtained for the peak position fit (Fig. 2).

Discussion

To understand the relationships between Raman spectral features and the Mg content of Mg–ACC shown in Figs 2 and 3, we first consider how Mg content influences the Raman spectra of calcite because the effect of Mg incorporation on the crystal structure is better understood. It is known in calcites that contain less than 25 mol % $MgCO_3$ that Mg substitutes for Ca and forms a solid solution.[29] Accommodation of the smaller Mg^{2+} ion causes significant disorder (strain) in the calcite structure (R-3c), resulting in a decrease in the average length of the metal–oxygen bond and a relative decrease in the length of the c-axis.[17] The decrease in the average metal–oxygen bond length is due to the presence of shorter Mg–O bonds (2.11 Å by Extended X-ray absorption fine structure (EXAFS)) compared with Ca–O bonds (2.39 Å by EXAFS).[8,30] Changes in metal–oxygen bond length have been

Table 2. Parameters to calculate the $MgCO_3$ content of ACC from carbonate ν_1 peak position or carbonate ν_1 FWHM, and the errors associated with calculations (cm^{-1})

Measurement	m	b	s_m	s_b
ν_1 peak position	0.2017	1079.66	0.0087	0.243
ν_1 FWHM	0.1964	23.40	0.0084	0.235

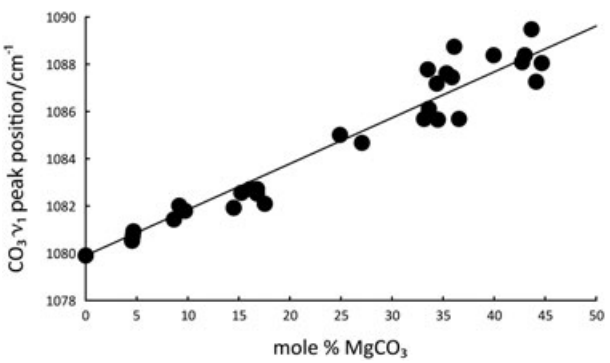

Figure 2. Carbonate ν_1 peak position *versus* $MgCO_3$ content of ACC (mol %). Line represents least squares fit with a R^2 value of 0.945.

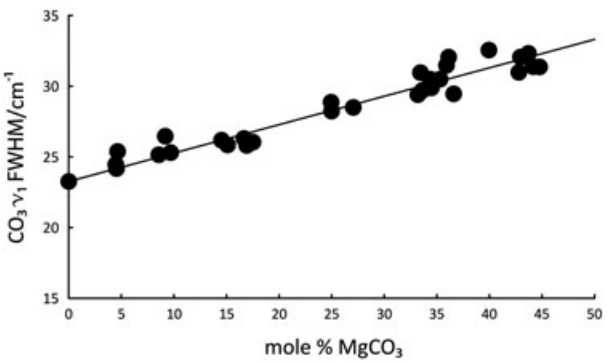

Figure 3. Carbonate ν_1 FWHM *versus* $MgCO_3$ content (mol %) of ACC. Line represents least squares fit with an R^2 value of 0.946.

attributed to differences in the polarizability of Ca *versus* Mg.[31] This difference in polarizability also controls Raman vibrational frequencies in the carbonate internal mode.[32]

The change in carbonate vibrational modes brought about by changes in metal–oxygen bond length is demonstrated in the ν_1 internal mode of free aqueous carbonate. This mode is predicted to be located at 1049 cm^{-1},[33] but experimental values measured from concentrated alkali carbonate solutions are centered between 1064 and 1069 cm^{-1}.[32] The effect of metal–oxygen bonding upon the ν_1 mode is demonstrated in the Raman spectra of calcite and magnesite, where the ν_1 position is red shifted from 1049 cm^{-1} (free carbonate ion) to 1085 cm^{-1} and 1094 cm^{-1}, respectively. The greater ν_1 red shift of magnesite compared with calcite is expected, as the shorter Mg–O bonds cause a greater change in carbonate C–O vibrational frequency.

For Mg-bearing calcites, Bischoff *et al.*[27] observed a continuous red shift and concurrent peak broadening for the carbonate ν_1 mode as $MgCO_3$ content increased from 0 to 25 mol %. In this case, the continuous red shift is indicative of random substitution in solid solution, where no phase separation occurs.[34] Bischoff *et al.* did not directly attribute the trend in peak broadening to the increase in the proportion of Mg–O bonds with increasing Mg substitution.[27] Peak broadening was instead interpreted in terms of Mg-induced positional disorder of the carbonate ion, an explanation that has been challenged in recent studies of Mg–calcites.[17,35] Although the exact cause of peak broadening may be disputed, it remains clear that random substitution of Mg for Ca in the calcite lattice increases the distribution of metal–oxygen bond lengths, a phenomenon known to increase Raman peak widths.[21]

We observed that changes in the Mg content of ACC caused both a red shift and peak broadening of the ν_1 carbonate symmetric stretch. Structurally, the order in the coordination environment about Ca in ACC is significantly decreased compared with calcite. Calcium is coordinated by 5–7 oxygen atoms in ACC, as determined by EXAFS, while Ca coordination in calcite is 6.[8] The absence of lattice modes in the spectra of ACC and broadening of the ν_1 peak in pure (0 mol % $MgCO_3$) ACC (FWHM = 22.5 cm^{-1}) compared with calcite (FWHM = 4.1 cm^{-1}) suggests that ACC represents a disordered solid. Such an interpretation is also supported by X-ray total scattering experiments showing that ACC contains 'local order' but lacks measurable order beyond 15 Å.[36]

Calcite, like all crystalline phases, exhibits long-range order, and the continuous shift in ν_1 peak position with increasing $MgCO_3$ content is considered to represent a substitutional solid solution.[27] The interpretation of the continuous ν_1 peak shift in Mg–calcite based on increases in the number of Mg–O bonds with random Mg substitution can be applied to the peak shifts observed in Mg-bearing ACC. The increase in ACC ν_1 peak width from 22.5 cm^{-1} (0 mol % $MgCO_3$) to 32 cm^{-1} (43 mol % $MgCO_3$) can be explained by the increased number of shorter Mg–O bonds in ACC.

We recognize that the ν_1 carbonate symmetric stretch shows spectral evidence of some asymmetry that becomes more pronounced as the peak broadens with increasing Mg contents (above 30 mol %) (Figs 1(c) and (d)). This observation suggests that the ν_1 peak could be a convolution of multiple discrete peaks, potentially invalidating the assumption that a solid solution model could explain the data. Recall that a single Gaussian–Lorentzian peak was used to fit the ν_1 peak. Because of the peak asymmetry, the data could (and possibly more correctly) also be fit to a more complex model that assumes the ν_1 peak consists of two (or more) discrete peaks. Although there is not enough reliable physical evidence to justify such an interpretation, it is known in calcium phosphate systems it can be hard to distinguish between a heterogeneous mixture of two different materials and a homogeneous solid solution.[37] The implication of using two or more peaks to fit the spectra would suggest that high-Mg–ACC could be described as a heterogeneous mixture of both ACC and an amorphous magnesium carbonate, rather than as a solid solution. Cryo–Transmission Electron Microscopy (Cryo–TEM) suggests that ACC is heterogeneous at the nanometer scale, and that the initial stage of ACC formation is the generation of 2 nm prenucleation clusters that subsequently aggregate and coalesce.[38] At high Mg concentrations, $MgCO_3$ prenucleation clusters may form and combine with $CaCO_3$ clusters. The resultant aggregates would contain discrete $MgCO_3$ and $CaCO_3$ domains and represent a physical mixture that would account for two ν_1 peaks. Although this is an intriguing and interesting concept, the possibility of a heterogeneous amorphous $MgCO_3 + CaCO_3$ mixture cannot be proven at this time and requires further investigation.

The findings herein show that the Mg content of ACC can be estimated based on the peak position or on the peak width of the Raman ν_1 carbonate symmetric stretch. The Raman technique thus provides a useful and reliable analytical tool to estimate Mg content in ACC of both synthetic and biological samples. This direct probe has the further advantage of providing a simple and nondestructive means of sample analysis that does not require extensive sample preparation beyond what is necessary for optical microscopy. The high spatial resolution of modern Raman microscopy offers a useful means of examining the Mg content of ACC within mineralizing specimens.

Acknowledgements

This research was funded by awards to PMD from the US Department of Energy (DOE BES-FG02-00ER15112) and the National Science Foundation (NSF OCE-1061763). DW thanks the Mineralogical Society of America for the Student Research Grant Award that also supported this work. We thank J. Donald Rimstidt for helpful discussions and the reviewers for insightful comments.

References

[1] L. Addadi, S. Raz, S. Weiner, *Adv Mat* **2003**, *15*, 959.
[2] D. B. Wang, A. F. Wallace, J. J. De Yoreo, P. M. Dove, *Proc Natl Acad Sci U S A* **2009**, *106*, 21511.
[3] E. Beniash, J. Aizenberg, L. Addadi, S. Weiner, *Proc R Soc London Ser B* **1997**, *264*, 461.
[4] I. M. Weiss, N. Tuross, L. Addadi, S. Weiner, *J Exp Zool* **2002**, *293*, 478.
[5] K. Benzerara, N. Menguy, P. Lopez-Garcia, T. H. Yoon, J. Kazmierczak, T. Tyliszczak, F. Guyot, G. E. Brown, *Proc Natl Acad Sci U S A* **2006**, *103*, 9440.
[6] J. Tao, D. Zhou, Z. Zhang, X. Xu, R. Tang, *Proc Natl Acad Sci U S A* **2009**, *106*, 22096.
[7] S. Weiner, I. Sagi, L. Addadi, *Science* **2005**, *309*, 1027.
[8] Y. Politi, Y. Levi-Kalisman, S. Raz, F. Wilt, L. Addadi, S. Weiner, I. Sagi, *Adv. Funct. Mater.* **2006**, *16*, 1289.
[9] Y. Politi, T. Arad, E. Klein, S. Weiner, L. Addadi, *Science* **2004**, *306*, 1161.
[10] F. C. Meldrum, H. Colfen, *Chem. Rev.* **2008**, *108*, 4332.
[11] S. Raz, P. C. Hamilton, F. H. Wilt, S. Weiner, L. Addadi, *Adv. Funct. Mater.* **2003**, *13*, 480.
[12] S. Raz, S. Weiner, L. Addadi, *Adv Mat* **2000**, *12*, 38.
[13] S. M. Stanley, *Chem. Rev.* **2008**, *108*, 4483.

[14] M. M. Tlili, M. Ben Amor, C. Gabrielli, S. Joiret, G. Maurin, P. Rousseau, *J Raman Spectrosc* **2001**, *33*, 10.
[15] C. Gunther, A. Becker, G. Wolf, M. Epple, *Zeitschrift Fur Anorganische Und Allgemeine Chemie* **2005**, *631*, 2830.
[16] A. A. Finch, N. Allison, *Mineral. Mag.* **2007**, *71*, 539.
[17] G. Falini, S. Fermani, M. Gazzano, A. Ripamonti, *J. Mater. Chem.* **1998**, *8*, 1061.
[18] W. D. Bischoff, F. C. Bishop, F. T. Mackenzie, *Am. Mineral.* **1983**, *68*, 1183.
[19] N. Rividi, M. van Zuilen, P. Philippot, B. Menez, G. Godard, E. Poidatz, *Astrobiology* **2010**, *10*, 293.
[20] T. Y. J. Han, J. Aizenberg, *Chem. Mater.* **2008**, *20*, 1064.
[21] F. Lin, A. K. Sum, R. J. Bodnar, *J Raman Spectrosc* **2007**, *38*, 1510.
[22] F. Lin, R. J. Bodnar, S. P. Becker, *Geochim Cosmochim Acta* **2007**, *71*, 3746.
[23] P. Verma, S. C. Abbi, K. P. Jain, *Physical Review B* **1995**, *51*, 16660.
[24] L. Nasdala, M. Wenzel, G. Vavra, G. Irmer, T. Wenzel, B. Kober, *Contrib. Mineral. Petrol.* **2001**, *141*, 125.
[25] H. Sumiya, N. Toda, Y. Nishibayashi, S. Satoh, *J Cryst Growth* **1997**, *178*, 485.
[26] P. K. Ajikumar, L. G. Wong, G. Subramanyam, R. Lakshminarayanan, S. Valiyaveettil, *Cryst Growth Des* **2005**, *5*, 1129.
[27] W. D. Bischoff, S. K. Sharma, F. T. Mackenzie, *Am. Mineral.* **1985**, *70*, 581.
[28] P. A. Schroeder, N. D. Melear, R. J. Pruett, *Appl Clay Sci* **2003**, *23*, 299.
[29] J. Paquette, R. J. Reeder, *Am. Mineral.* **1990**, *75*, 1151.
[30] Y. Politi, D. R. Batchelor, P. Zaslansky, B. F. Chmelka, J. C. Weaver, I. Sagi, S. Weiner, L. Addadi, *Chem. Mater.* **2009**, *22*, 161.
[31] M. H. Booker, M. A. Bredig, *J. Chem. Phys.* **1973**, *58*, 5319.
[32] W. B. White, in *The Infra-red Spectra of the Minerals (Ed.: V. C. Farmer), Mineralogical Society, London,* ***1974****, pp. 227.*
[33] J. T. Kloprogge, D. Wharton, L. Hickey, R. L. Frost, *Am. Mineral.* **2002**, *87*, 623.
[34] W. B. White, in *The Infra-red Spectra of the Minerals (Ed.: V. C. Farmer), Mineralogical Society, London,* ***1974****, pp. 87.*
[35] E. Zolotoyabko, E. N. Caspi, J. S. Fieramosca, R. B. Von Dreele, F. Marin, G. Mor, L. Addadi, S. Weiner, Y. Politi, *Cryst Growth Des* **2010**, *10*, 1207.
[36] F. M. Michel, J. MacDonald, J. Feng, B. L. Phillips, L. Ehm, C. Tarabrella, J. B. Parise, R. J. Reeder, *Chem. Mater.* **2008**, *20*, 4720.
[37] J. D. Pasteris, D. Y. Ding, *Am. Mineral.* **2009**, *94*, 53.
[38] E. M. Pouget, P. H. H. Bomans, J. Goos, P. M. Frederik, G. de With, N. Sommerdijk, *Science* **2009**, *323*, 1555.